Site-Dependent Eu 3+ Photoluminescence in Double Perovskite-Type Alkaline Earth Lanthanum Tantalates

Kazushige Ueda, Takuma Yoshino, Yuhei Shimizu, Tetsuo Honma, Florian Massuyeau, Stéphane Jobic

Site-Dependent Eu^{3+} Photoluminescence in Double Perovskite-Type Alkaline Earth Lanthanum Tantalates

Kazushige Ueda[*,†], *Takuma Yoshino*[†], *Yuhei Shimizu*[‡], *Tetsuo Honma*[⊥], *Florian Massuyeau*[§], *and Stéphane Jobic*[§]

[†]Department of Materials Science, Graduate School of Engineering, Kyushu Institute of Technology, 1-1 Sensui, Tobata, Kitakyushu 804-8550, Japan.

[‡]National Metrology Institute of Japan (NMIJ), National Institute of Advanced Industrial Science and Technology (AIST), 1-1-1 Umezono, Tsukuba, Ibaraki 305-8563, Japan

[⊥]Japan Synchrotron Radiation Research Institute, 1-1-1 Kouto, Sayou-cho, Sayou-gun, Hyogo 679-5198, Japan

[§]Université de Nantes, CNRS, Institut des Matériaux Jean Rouxel, IMN, F-44000 Nantes, France

[*] Corresponding author

Highlights

1. Phase-pure Eu^{3+} doped Ca_2LaTaO_6 (CLTO) and Ba_2LaTaO_6 (BLTO) were prepared.

2. Eu^{3+} were confirmed to be at A sites in CLTO and B sites in BLTO by XANES analysis.

3. Eu^{3+} site-dependent PL spectra were obtained using the Eu^{3+}-site-confirmed samples.

4. Site-dependent PL and the lifetime were examined systematically by CT excitation.

5. High external efficiency of 28% was found in the Eu^{3+} doped BLTO double perovskite.

ABSTRACT

Site-dependent Eu^{3+} photoluminescence (PL) was examined utilizing the structural difference of two Eu^{3+} doped alkaline earth lanthanum tantalates with the B-site-ordered double perovskite-type structure (AA')[BB']O_6, viz. $(CaLa_{1-x}Eu_x)[CaTa]O_6$ (CLTO:Eu^{3+}) and $(Ba_2)[La_{1-x}Eu_xTa]O_6$ (BLTO:Eu^{3+}) (x = 0.01, 0.10). The locations of the Eu^{3+} ions were experimentally determined by X-ray absorption near edge structure of the Eu L_{III} edge and confirmed to be A sites in CLTO:Eu^{3+} and B sites in BLTO:Eu^{3+} as expected from the nominal compositions. Intense charge transfer (CT) excitation bands were observed in the UV region in the PL excitation spectra of both materials. Because of the shorter bond lengths and larger electronic repulsion at B sites than A sites, the CT excitation band of Eu^{3+} at B sites in BLTO:Eu^{3+} was blue-shifted compared to that of Eu^{3+} at A sites in CLTO:Eu^{3+}. By UV excitation in the CT bands, both materials showed red luminescence. However, due to the difference in the site symmetry of A and B sites, the Eu^{3+} emission was mainly derived from the $^5D_0$ – $^7F_2$ transitions in CLTO:Eu^{3+} and from the $^5D_0$ – $^7F_1$ transitions in BLTO:Eu^{3+} in relation with Eu^{3+} at A and B sites, respectively. The lifetimes of the emission were also dependent on the Eu^{3+} sites resulting in the longer lifetimes of Eu^{3+} ions at B sites than those at A sites.

KEYWORDS: Eu^{3+} emission, site-dependent luminescence, double perovskite, alkaline earth lanthanum tantalates

INTRODUCTION

Lanthanide (Ln) ions are frequently doped in various host lattices (HLs) and used as activators in luminescent materials taking advantage of the 4f–4f and 5d–4f electronic transitions.[1-3] Because the sizes of the Ln ions are relatively large, they are usually substituted for large cations such as La, Y, Ba, Sr and Ca ions.[4] In the HLs of simple perovskite-type oxides (ABO_3), these large cations are basically located at A sites accompanying smaller cations such as transition metal ions at B sites.[5] Therefore, in many cases, luminescence properties of Ln doped simple perovskite-type oxides reported in literatures are derived from Ln ions located at A sites. Accordingly, the luminescence properties of Ln ions at B sites have not been investigated sufficiently so far. Even though the study on the B-site luminescence is intended, the doping of large Ln ions at B site is basically difficult in the simple perovskite-type oxides for steric reasons. This can be simply understood from the Goldschmidt's tolerance factor, which gives a criterion of the stability of the perovskite-type structure. [6]

In contrast to the simple perovskite-type oxides, double perovskite-type oxides, which can be expressed by the formula of $(AA')[BB']O_6$, have a more wide diversity of the combinations of cations in the viewpoints of both their valence and sizes.[7-9] This is because two ions at each site, A and A' or B and B', can be chosen separately and taken into account for the structural stability. Alkaline earth lanthanum tantalates, Ca_2LaTaO_6 (CLTO) and Ba_2LaTaO_6 (BLTO), are typical examples; La^{3+} ions occupy A sites randomly with Ca^{2+} ions in CLTO as expressed by $(CaLa)[CaTa]O_6$, whereas La^{3+} ions can inhabit B sites alternately with Ta^{5+} ions in BLTO as indicated by $Ba_2[LaTa]O_6$.[10-12] Therefore, each La^{3+} ion is coordinated by eight O^{2-} ions at A site in CLTO and six O^{2-} ions at B site in BLTO. The crystal structures of CLTO and BLTO are shown in Figure 1.

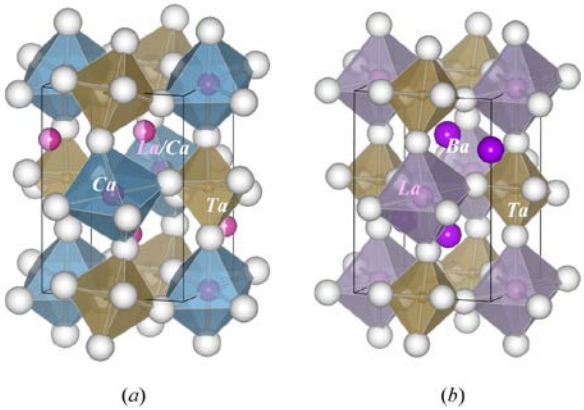

Figure 1. Crystal structures of (a) Ca_2LaTaO_6 and (b) Ba_2LaTaO_6 with double perovskite structure. La ions are located at A sites in (CaLa)[CaTa]O_6 and at B sites in Ba_2[LaTa]O_6.

Eu^{3+} ions are widely used as activators for red or red-orange luminescence originating from $^5D_0$ – ^7F_J electronic transitions. In addition, among the Ln ions, Eu^{3+} ions are especially known to show clear site-dependent luminescence; the induced electronic dipole (ED) transitions from $^5D_0$ to $^7F_2$ states are mainly observed at a site without inversion symmetry, while the magnetic dipole (MD) transitions from $^5D_0$ to $^7F_1$ states are predominantly seen at a site with inversion symmetry.[13,14] In the crystal structures of CLTO and BLTO, the site-symmetry for La sites is 1 without inversion symmetry in CLTO and $\bar{1}$ with inversion symmetry in BLTO. Consequently, distinguishable Eu^{3+} emissions are anticipated between Eu^{3+} doped CLTO (CLTO:Eu^{3+}) and BLTO (BLTO:Eu^{3+}) if Eu^{3+} are substituted at La sites as intended.

Many Eu^{3+} doped double perovskite-type oxides have been already reported to show red or red-orange luminescence.[15-40] Nevertheless, data on the site-dependent photoluminescence (PL) of Eu^{3+} in these host lattices (HLs) are still limited[15-18] In particular, comprehensive comparisons of Eu^{3+} PL characteristics between A and B sites and the fluorescence lifetimes have been hardly discussed systematically. In some reports, Eu^{3+} PL properties in several double perovskite-type oxides were studied, but the site-dependence and the lifetime were not primarily concerned. In

other contributions, Eu^{3+} ions were excited differently either via HL, charge transfer (CT) bands or 4f–4f transitions, which possibly resulted in different PL spectral shapes and lifetimes. Therefore, the site-dependent Eu^{3+} PL properties in the double perovskite-type oxides have not been completely understood yet.

In our previous study, the site-dependent Eu^{3+} PL was examined in the simple perovskite-type oxide of $LaLuO_3$ doped with Eu^{3+} at A and B sites ($LaLuO_3$:Eu^{3+}(A) and $LaLuO_3$:Eu^{3+}(B), respectively).[41] Although the differences of the spectral shapes between $LaLuO_3$:Eu^{3+}(A) and $LaLuO_3$:Eu^{3+}(B) were evidently observed depending on the Eu^{3+} sites, some mixed luminescence from both A and B sites were observed, especially in B-site doped samples at high Eu^{3+} concentration. In this study, the PL and PLE properties of CLTO:Eu^{3+} and BLTO:Eu^{3+} were examined in details to observe individual Eu^{3+} PL from A or B sites more clearly taking advantage of the structural difference in these double perovskite-type oxides. The location of Eu^{3+} ions were surely determined by the X-ray absorption near edge structures (XANES) of the Eu L_{III} absorption edge. The site-dependent PL spectra and the lifetimes were obtained from Eu^{3+} ions, which were commonly excited via CT bands.[42]

EXPERIMENTS

The samples of CLTO:Eu^{3+} and BLTO:Eu^{3+} were prepared by the conventional solid state reaction. The nominal compositions of the samples are $(CaLa_{1-x}Eu_x)[CaTa]O_6$ for CLTO:Eu^{3+} and $Ba_2[La_{1-x}Eu_xTa]O_6$ for BLTO:Eu^{3+} (x = 0.01, 0.10). Starting materials of $CaCO_3$ or $BaCO_3$, La_2O_3, Ta_2O_5, and Eu_2O_3 (Kojundo Chemical Laboratory Co., Ltd., 99.9%) were weighed in stoichiometric amount and thoroughly mixed with ethanol in an agate mortar. The mixed

powders were dried and shaped into pellets, and heated at 1300 ℃ for 6 h in air. The pellets were then finely ground, powders were pressed into pellets again and heated at 1400 ℃ for 6 h in air. Nondoped samples (x = 0.00) were also prepared similar way to determine the absorption edges of the HLs.

X-ray diffraction (XRD) measurements were carried out using an X-ray diffractometer with a rotary Cu target (Rigaku, RINT-2500). The powder XRD patterns for the pure crystalline phases were simulated using the RIETAN code,[43] and the images of their crystal structures were depicted using the VESTA code.[44] The spectra of X-ray absorption near edge structures (XANES) at the Eu L_{III} edges were measured at the BL14B2 beamline of the SPring-8 synchrotron radiation facility. The XANES spectra of the samples with x = 0.10 were obtained along with those of reference samples of $EuAlO_3$ and $Ba_2[EuTa]O_6$. The PL and PLE spectra of the samples were measured at room temperature (RT; 298 K) and liquid nitrogen temperature (LNT; 77 K) using conventional spectrofluorometers (JASCO FP-6500 and Horiba Fluorolog-3). The decay curves of Eu^{3+} PL peaks were examined to estimate the lifetimes for Eu^{3+} at A and B sites. The quantum efficiencies of Eu^{3+} PL derived from A and B sites were also evaluated at RT using an integrating sphere.

RESULTS AND DISCUSSION

The XRD patterns of the samples, $(CaLa_{1-x}Eu_x)[CaTa]O_6$ and $Ba_2[La_{1-x}Eu_xTa]O_6$ (x = 0.00, 0.01, 0.10), are shown in Figure 2. All samples are phase pure and no secondary phases are detected. Magnified diffraction peaks are shown in insets to clarify peak shifts induced by Eu^{3+} substitution at La sites. The peak shifts are clearly seen for the samples of x =0.10 in both

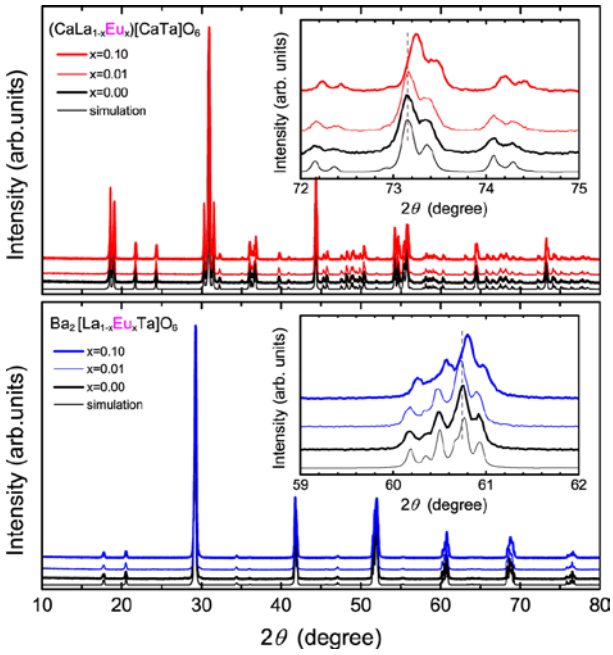

Figure 2. XRD patterns of (top) $(CaLa_{1-x}Eu_x)[CaTa]O_6$ and (bottom) $Ba_2[La_{1-x}Eu_xTa]O_6$ (x = 0.00, 0.01, 0.10) along with those simulated from the structural data. Magnified diffraction peaks at high 2θ angles are shown in insets.

CLTO:Eu^{3+} and BLTO:Eu^{3+}. The peak shifts to higher angles suggest the decrease of the lattice spacing due to the substitution of Eu^{3+} for La^{3+}. These results are reasonable because the ionic radii of Eu^{3+} ions (r_{VIII} = 1.206 Å at A sites, r_{VI} = 1.087 Å at B sites) are smaller than those of La^{3+} ions (r_{VIII} = 1.300 Å, r_{VI} = 1.172 Å).[4]

The locations of Eu^{3+} ions in the crystal structures were determined by XANES measurements. The spectra of XANES at the Eu L_{III} edges for CLTO: Eu^{3+} and BLTO: Eu^{3+} are depicted in Figure 3. Perovskite-type $EuAlO_3$ and double perovskite-type $Ba_2[EuTa]O_6$ were used as references for Eu^{3+} at A site and B site, respectively.[11, 45] Because the Eu L_{III} absorption is primarily derived from electronic transitions from 2p to 5d states, the shape of the intense L_{III} absorption peaks denotes the densities of the empty Eu^{3+} 5d states, which enable us to identify the crystal sites occupied by the Eu^{3+} ions. [46, 47]

$EuAlO_3$ shows an intense single peak at 6979 eV, whereas $Ba_2[EuTa]O_6$ does a main peak at 6981 eV with a shoulder at 6978 eV. The positions of two broad peaks observed at higher energy are also different for the two compounds, located at 6991 and 7010 eV for $EuAlO_3$ and at 6997 and 7019 eV for $Ba_2[EuTa]O_6$. The shoulder peak of the main peak observed in $Ba_2[EuTa]O_6$ can be regarded as a consequence of the splitting of the empty Eu^{3+} 5d states under the influence of the crystal field. This splitting is expected to be significantly larger for Eu^{3+} ions at small octahedral B sites than at large cuboctahdral A sites. Namely, an energy splitting as large as ca. 3 eV can be envisioned for $Ba_2[EuTa]O_6$ with the average Eu−O bond length of 2.26 Å, which is much shorter than that in $EuAlO_3$ (d_{Eu-O} = 2.46 Å). [11, 45]

CLTO:Eu^{3+} gives a main single peak at E = 6979 eV and two broad peaks at higher energy, indicating the location of Eu^{3+} at A sites as in $EuAlO_3$. BLTO:Eu^{3+} provides a spectral shape similar to that of $Ba_2[EuTa]O_6$ with a double peak at 6981 and 6978 eV, which endorses Eu^{3+} ions at B sites. These observations of Eu^{3+} local structures directly revealed the locations of Eu^{3+} ions in CLTO and BLTO HLs.

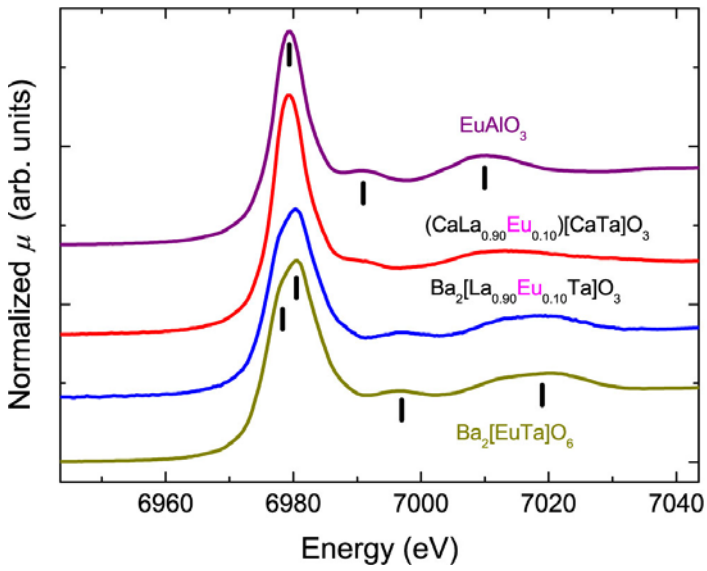

Figure 3. XANES spectra of Eu L_{III} edges for $(CaLa_{0.90}Eu_{0.10})[CaTa]O_6$ and $Ba_2[La_{0.90}Eu_{0.10}Ta]O_6$ samples along with those for $EuAlO_3$ and $Ba_2[EuTa]O_6$ references.

Figure 4 shows PL and PLE spectra of CLTO:Eu^{3+} 10% and BLTO:Eu^{3+} 10% along with the absorption (Abs) spectra of CLTO and BLTO HLs. The spectral features for the Eu concentration of x = 0.01 were almost the same with those for x = 0.10. Going from x = 0.01 to x = 0.10, PL intensities increase simply and BLTO:Eu^{3+} systematically exhibited higher PL intensities than CLTO:Eu^{3+}. To achieve a systematic understanding of site-dependent Eu^{3+} PL, Eu^{3+} ions were directly excited through the CT from O^{2-} to Eu^{3+} in both CLTO:Eu^{3+} and BLTO:Eu^{3+} as previously done in $LaLuO_3$:Eu^{3+}.[41]

Based on the examination of the CLTO absorption spectrum, the absorption threshold of the CLTO HL is estimated to be at 240 nm. The PLE spectrum of CLTO:Eu^{3+}, monitoring the PL peak at 614 nm, shows an intense broad band centered at 298 nm and several sharp peaks in the 360–420 nm range. The former intense band can be unambiguously assigned to the CT transitions, and the latter is to Eu^{3+} intraconfigurational 4f–4f ones. Let us notice that the position

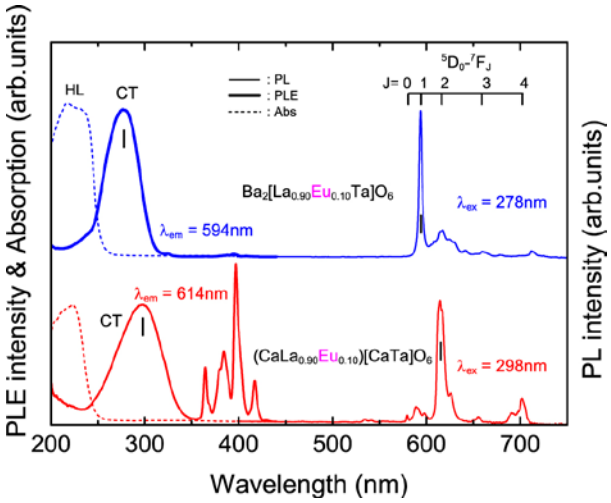

Figure 4. PL and PLE spectra of $(CaLa_{0.90}Eu_{0.10})[CaTa]O_6$ (red lines) and those of $Ba_2[La_{0.90}Eu_{0.10}Ta]O_6$ (blue lines) samples along with absorption spectra of pure HL samples. PL, PLE, and Abs spectra are drawn with thin lines, thick lines and dashed lines, respectively.

of the CT excitation band (λ_{ex} = 298 nm) in CLTO:Eu^{3+} is very close to that (λ_{ex} = 292 nm) in $LaLuO_3$:Eu^{3+}(A).[41] This may originate from almost identical average Eu−O bond length at A sites, regarding the Eu−O bond length as La−O one, i.e. 2.61 Å for CLTO and 2.66 Å and for $LaLuO_3$. Formally, CT excitation bands for La perovskite-type HLs with Eu^{3+} activators at A sites, such as $LaAlO_3$ (d_{La-O} = 2.68 Å) and $LaGaO_3$ (d_{La-O} = 2.65 Å), are observed at analogous wavelengths (310 and 303 nm, respectively).[42,45,48,49] The PL spectrum of CLTO:Eu^{3+} obtained by the CT excitation at 298 nm consists of an intense peak at 614 nm that derives from the $^5D_0$ – $^7F_2$ transitions. The excitation through a 4f–4f transition at 397 nm did not lead to any significant change in the PL spectral features in comparison with the CT excitation.

The absorption spectrum of BLTO reveals an absorption edge at 250 nm. The PLE spectrum of BLTO:Eu^{3+}, monitored at 594 nm, shows an intense broad band at 278 nm. Accordingly, the intense band is associated with the CT transition. The 4f–4f excitation peaks in BLTO: Eu^{3+} are negligible and much less intense than those observed in CLTO:Eu^{3+}. This stems from the forbidden character of the 4f–4f ED transitions for Eu^{3+} at the B sites in contrast with partly permitted 4f–4f ED transitions for Eu^{3+} at the A sites. Moreover, the CT excitation band in BLTO:Eu^{3+} appears at shorter wavelengths than that in CLTO:Eu^{3+} (278 vs. 298 nm). This result is consistent with the one that the CT band for Eu^{3+} at B sites is observed at shorter wavelengths than that for Eu^{3+} at A sites in Eu^{3+} doped $LaLuO_3$.[41] The blue-shift of the CT band for Eu^{3+} ions at B sites is attributed to the shorter Eu – O bond lengths at B sites in BLTO:Eu^{3+} ($d_{La(Eu)–O}$ = 2.43 Å) than at A sites in CLTO:Eu^{3+} ($d_{La(Eu)–O}$ = 2.61 Å). Namely, Coulomb repulsion between electrons in Eu 4f orbitals and those in O 2p orbitals becomes larger at B sites resulting in the uplifted energy of the CT states. It is noteworthy that the blue-shift of the CT excitation peak in BLTO:Eu^{3+} is not as large as that observed in $LaLuO_3$:Eu^{3+} (B) (λ_{ex} = 230 nm). This is because

the Eu – O bond lengths in BLTO:Eu^{3+} is not as short as those in $LaLuO_3$:Eu^{3+}(B) ($d_{Lu(Eu)-O}$ = 2.22 Å). The PL spectrum recorded at λ_{ex} = 278 nm consists mainly of the peak at 594 nm assigned to the $^5D_0$ – $^7F_1$ transitions. The PL spectral shapes are largely different between CLTO:Eu^{3+} and BLTO:Eu^{3+} and the details are discussed below.

The PL peaks in CLTO:Eu^{3+} and BLTO:Eu^{3+} obtained by the CT excitation at RT and LNT are magnified in Figure 5. In the CLTO:Eu^{3+}, Eu^{3+} ions at A sites without the inversion symmetry make the PL for the $^5D_0$ – $^7F_2$ induced ED transitions dominant and the PL for the $^5D_0$ – $^7F_4$ transitions secondly dominant. The weak single PL peak for the $^5D_0$ – $^7F_0$ transition and three peaks for the $^5D_0$ – $^7F_1$ transitions are seen although they are forbidden originally. In the BLTO:Eu^{3+}, Eu^{3+} ions at B sites with the inversion symmetry drive the PL for the $^5D_0$ – $^7F_1$ MD transitions predominant and the PL for the $^5D_0$ – $^7F_0$ transition almost absent. These features are very similar to the Eu^{3+} luminescence observed in Ba_2MgWO_6:Eu^{3+}, $Ba_2La_{2/3}TeO_6$:Eu^{3+} and Ba_2GdNbO_6:Eu^{3+}.[25-27] The single PL peak for the $^5D_0$ – $^7F_0$ transition can be recognized at LNT by further magnification. The red-shift or larger splitting for the $^5D_0$ – $^7F_4$ transition peaks is also observed in BLTO:Eu^{3+}, which is probably attributed to the differences in spin-orbital coupling and crystal field between A and B sites.

The single peak of the $^5D_0$ – $^7F_0$ transition at different wavelength in CLTO:Eu^{3+} (580 nm) and BLTO:Eu^{3+} (581 nm) confirms the single site of Eu^{3+} in each material.[50] The peak splitting for the $^5D_0$ – $^7F_1$ transition is clearly seen in CLTO:Eu^{3+} but not in BLTO:Eu^{3+}. Taking the site symmetry into account, the triple splitting in CLTO:Eu^{3+} is reasonable for Eu^{3+} at A sites with the low site symmetry of 1.[13, 14] The site symmetry of B sites in BLTO is $\bar{1}$ and low enough to give the peak splitting, but it is hardly observed in BLTO:Eu^{3+}. Two possibilities are considered to explain the absence of the splitting. One is that the splitting is too small to detect for the

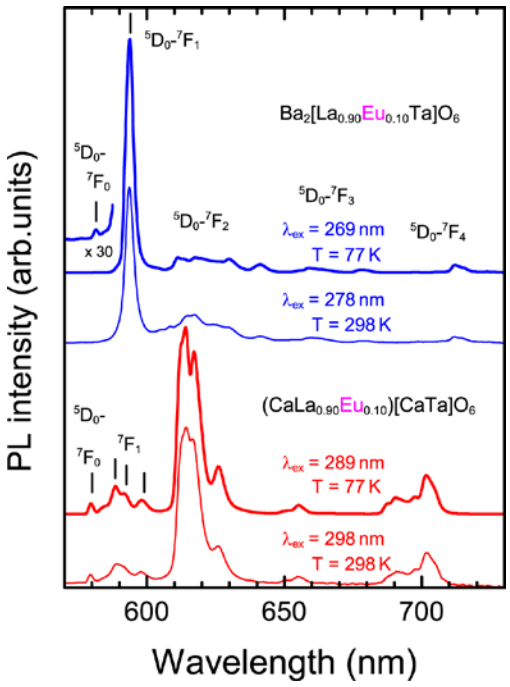

Figure 5. Magnified PL spectra of $(CaLa_{0.90}Eu_{0.10})[CaTa]O_6$ (red lines) and those of $Ba_2[La_{0.90}Eu_{0.10}Ta]O_6$ (blue lines) obtained by the CT excitation at RT (thin lines) and LNT (thick lines).

spectrometer used in this study. The other is that the local structural relaxation around Eu^{3+} ions at B sites occurs and makes the Eu^{3+} site symmetry very high because the distortion of the B-site octahedron is originally small in BLTO and $Ba_2[EuTa]O_6$. In comparison with the spectral shape of Ba_2MgWO_6:Eu^{3+},[25] the latter seems to be more presumable. As for the temperature dependence of spectral shapes, the peaks in the spectra for both materials become sharper at LNT than at RT, but the spectral features are unchanged. This results indicates the doped Eu^{3+} ions are distributed homogeneously and they are isolated enough to provide the individual Eu^{3+} PL from A or B sites in each HL. Therefore, the mixing of the Eu^{3+} PL from A and B sites is not observed at RT and LNT in these double perovskite-type HLs, which contrasts with the simple perovskite-type HL of $LaLuO_3$.[41]

The decay curves of the PL peaks for the $^5D_0 - {}^7F_2$ transitions in CLTO:Eu^{3+} and those for the $^5D_0 - {}^7F_1$ transitions in BLTO:Eu^{3+} obtained by excitation via the CT bands are shown in Figure 6. The main peak at 614 nm for CLTO:Eu^{3+} derived from the induced ED transitions and the intense peak at 594 nm for BLTO:Eu^{3+} derived from the MD transitions were examined at RT and LNT. It was found obviously that the Eu^{3+} PL from A sites in CLTO:Eu^{3+} shows much faster decay than that from B sites in BLTO:Eu^{3+}. This result is very similar to that observed in the simple perovskite-type oxide of $LaLuO_3$ doped with Eu^{3+} at A and B sites.[41] The faster decay at A sites than at B sites is basically attributed to that the probability of the induced ED transitions is usually higher than that of the MD transitions. The transition probability will be dependent on not only the site symmetry but also the local structures such as bond lengths and coordination numbers.

The decay curves for CLTO:Eu^{3+} are not largely dependent on the temperatures between RT and LNT, whereas those for BLTO:Eu^{3+} showed conspicuous temperature dependence implying

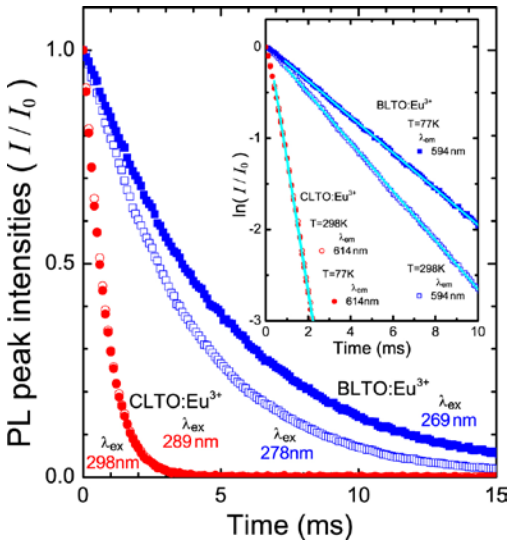

Figure 6. Decay curves of PL peak intensities for $(CaLa_{0.90}Eu_{0.10})[CaTa]O_6$ (red circle symbols) and those for $Ba_2[La_{0.90}Eu_{0.10}Ta]O_6$ (blue square symbols) observed under CT excitation at RT (open symbols) and LNT (filled symbols).

that the Eu^{3+} PL from B sites is largely influenced by the lattice vibrations. Although these results are similar to the Tb^{3+} doped samples reported previously,[51] the temperature dependence for the present Eu^{3+} doped samples is notably larger than the one for the Tb^{3+} doped samples. The B–O bonds in the perovskite-type ABO_3 are much shorter and generally have more covalent character than the A–O bonds. [52] In addition, the BO_6 octahedra are three-dimensionally connected sharing corners in simple or double perovskite-type oxides. Therefore, the larger influence of the lattice vibration on the B-site luminescence seems to be reasonable. The valence states of Eu ions become to be divalent just after the CT excitation and their ionic sizes increase, whereas the valence states of Tb ions are the same after the 4f-5d excitation. The differences in the excited states between Eu and Tb ions are probably attributed to the larger temperature dependence for the Eu ions at B sites.

The lifetimes (τ) for the Eu^{3+} PL derived from the $^5D_0 - {}^7F_1$ and $^5D_0 - {}^7F_2$ transitions were estimated by the plots of $ln(I/I_0)$ vs. t as shown in the inset presuming that the decay curves follow a single-exponential function. The slopes in the inset provide the lifetimes τ = 0.69 ms for the $^5D_0 - {}^7F_2$ transitions both at RT and LNT in CLTO:Eu^{3+} and τ = 3.7 ms for the $^5D_0 - {}^7F_1$ transitions at RT and τ = 5.1 ms at LNT in BLTO:Eu^{3+}. These values were obtained by the direct excitation of Eu^{3+} through the CT transitions. The evaluation of the lifetimes was also carried out by the direct Eu^{3+} excitation through 4f–4f transitions at 395 or 397 nm. The results were almost the same with those by the CT excitation, indicating the relaxation from the excited CT states (Eu^{2+} states) to the excited Eu^{3+} $^5D_0$ states is far much faster than the relaxation from the $^5D_0$ to ^7F_J states.

Although the lifetimes of Eu^{3+} PL in the double perovskite-type oxides have been reported in several papers,[22-38] Eu^{3+} sites and the excitation wavelengths have not been examined systematically for the understanding of the site-dependent Eu^{3+} luminescence. Therefore, it is limited to compare the lifetimes among the double perovskite-type oxides. The present results were roughly the same with τ = 0.5 ms in $Ca_2LaTaO_6:Eu^{3+}$, τ = 0.69 ms in $Ca_2LuTaO_6:Eu^{3+}$ and τ = 0.61 ms in $Gd_2ZnTiO_6:Eu^{3+}$ for Eu^{3+} ions at A sites, and τ = 4.23 ms in $Ba_2MgWO_6:Eu^{3+}$ and τ = 3.55 ms in $Ba_2La_{2/3}Te_{1/3}O_6:Eu^{3+}$ for those at B sites. [22-26]

The quantum efficiencies (η) of the Eu^{3+} PL were evaluated at RT for excitation via the CT peaks, namely, at 298 nm for CLTO:Eu^{3+} and at 278 nm for BLTO:Eu^{3+}, using all emission peaks in the visible region. The internal quantum efficiency (η_{in}) and external quantum efficiency (η_{ex}) for CLTO:Eu^{3+} (x=0.10) were 8 and 5 %, respectively, which were lower than those for $LaLuO_3:Eu^{3+}$(A). In contrast, those values for BLTO:Eu^{3+} (x=0.10) were η_{in} = 39 and η_{ex} = 28 %, which were higher than those for $LaLuO_3:Eu^{3+}$(B) (η_{in} = 34 and η_{ex} = 27 %).[41] Between the two double perovskite-type materials, Eu^{3+} at B sites in BLTO:Eu^{3+} provided higher efficiency than that at A sites in CLTO:Eu^{3+}. The dominant Eu^{3+} luminescence at B sites is also observed in the double perovskite-type $Sr_2CaMo_{1-y}W_yO_6$ doped with Eu^{3+} at A or B sites.[17] On the other hand, the efficiency is comparable between A and B sites in the simple perovskite-type $LaLuO_3$.[41] Because the η_{ex} values are dependent on the HLs, excitation wavelengths, Eu^{3+} concentrations, grain sizes and so on, it is not simple to compare them in details. In the other double perovskite-type oxide hosts for the application to white light emitting diodes, several η values have been reported; η = 17.8 % (λ_{ex} = 395 nm), 27.7% (λ_{ex} = 534 nm) for $Ca_2La_{0.6}Eu_{0.4}NbO_6$, η = 20.4 % (λ_{ex} = 395 nm), 25.4% (λ_{ex} = 465 nm) for

$Sr_2Ca(Mo_{0.5}W_{0.5})O_6:Eu_{0.04}$ and η = 17 % (λ_{ex} = 390 nm) for $Sr_2Ca_{0.7}Eu_{0.15}Li_{0.15}W_{0.5}Mo_{0.5}O_6$.[15, 17, 40]

CONCLUSION

The Eu^{3+} luminescence of B-site-ordered double perovskite-type $(CaLa_{1-x}Eu_x)[CaTa]O_6$ and $Ba_2[La_{1-x}Eu_xTa]O_6$ (x = 0.01, 0.10) were investigated based on the experimental examination of Eu^{3+} locations. XANES measurements confirmed that Eu^{3+} ions are located at A sites in CLTO:Eu^{3+} and at B sites in BLTO:Eu^{3+} as expected in the nominal compositions. In the PLE spectra, broad CT excitation bands were observed in both CLTO:Eu^{3+} and BLTO:Eu^{3+} revealing the blue shift of the CT band for BLTO:Eu^{3+} compared with CLTO:Eu^{3+} due to the larger crystal field at B sites. Although both materials showed red PL, the PL spectral shapes were largely different depending on the Eu^{3+} occupation sites accompanying the difference of the PL lifetimes. Eu^{3+} ions at A sites without the inversion symmetry in CLTO:Eu^{3+} provide the intense PL peak derived from the $^5D_0 - {}^7F_2$ transition, whereas those at B sites with the inversion symmetry in BLTO:Eu^{3+} give the sharp PL peak derived from the $^5D_0 - {}^7F_1$ transition. As a result, evident site-dependent Eu^{3+} PL and the lifetimes were obtained in these double perovskite-type oxides clarifying the spectral shape of each Eu^{3+} PL from A or B site.

ACKNOWLEDGMENT

This work was partly supported by the Japan Society for the Promotion of Science (JSPS) KAKENHI (Grant JP16K06724 and JP19K05004). The synchrotron radiation experiments were

performed at beamline BL14B2 of SPring-8 with the approval of the Japan Synchrotron Radiation Research Institute (JASRI; Proposal 2017B1576 and 2018B1573).

REFERENCES

[1] W. M. Yen, S. Shionoya, H. Yamamoto Eds., Phosphor Handbook, CRC Press, Boca Raton, FL, 2006.

[2] G. Blasse, B. C. Grabmaier, Luminescent Materials, Springer-Verlag, Berlin, 1994.

[3] A. Kitai, Ed. Luminescent Materials and Applications, John Wiley & Sons, Chichester, 2008.

[4] R. D. Shannon, Revised effective ionic radii and systematic studies of interatomic distances in halides and chalcogenides, Acta Crystallogr. A32 (1976) 751−767.

[5] R. S. Roth, Classification of Perovskite and Other ABO_3-Type Compounds, J. Res. Nat. Stand. 58 (1957) 75−88.

[6] V. M. Goldschmidt, Die Gesetze der Krystallochemie, Naturwissenschaften 14 (1926) 477−485.

[7] S. Vasala, M. Karppinen, $A_2B'B''O_6$ perovskites: A review, Prog. Solid State Chem. 43 (2015) 1−36.

[8] A. Hossain, P. Bandyopadhyay, S. Roy, An overview of double perovskites $A_2B'B''O_6$ with small ions at A site: Synthesis, structure and magnetic properties, J. Alloys Compd. 740 (2018) 414−427.

[9] G. Volonakis, N. Sakai, H. J. Snaith, F. Giustino, Oxide analogs of halide perovskites and the new semiconductor Ba_2AgIO_6, J. Phys. Chem. Lett. 10 (2019) 1722−1728.

[10] V. K. Trunov, L. I. Konstantinova, A. A. Evdokimov, The X-ray analysis of the compounds Ca_2LnTaO_6, Russ. J. Inorg. Chem. 28 (1983) 807-809. ; A. Dutta, S. Saha, P. Kumari, T. P. Sinha, S. Shannigrahi, Crystal structure and X-ray photoemission spectroscopic study of A_2LaMO_6 [A=Ba, Ca; M=Nb, Ta], J. Sold State Chem. 229 (2015) 296−302.

[11] Y. Doi, Y. Hinatsu, Magnetic properties of ordered perovskites Ba_2LnTaO_6 (Ln = Y, lanthanides), J. Phys.: Condens. Matter. 13 (2001) 4191−4202.

[12] P. J. Saines, J. R. Spencer, B. J. Kennedy, M. Avdeev, Structures and crystal chemistry of the double perovskites $Ba_2LnB'O_6$ (Ln = lanthanide B'= Nb^{5+} and Ta^{5+}): Part I. Investigation of Ba_2LnTaO_6 using synchrotron X-ray and neutron powder diffraction, J. Solid State Chem. 180 (2007) 2991−3000.

[13] K. Binnemans, Interpretation of europium(III) spectra, Coordin. Chem. Rev. 295 (2015) 1−45

[14] G. Blasse, A. Bril, W. C. Nieuwpoort, On the Eu^{3+} fluorescence in mixed metal oxides, J. Phys. Chem. Solids. 27 (1966) 1587−1592.

[15] X. Yin, Y. Wang, F. Huang, Y. Xia, D. Wan, J. Yao, Excellent red phosphors of double perovskite Ca_2LaMO_6:Eu (M=Sb, Nb, Ta) with distorted coordination environment, J. Solid State Chem. 184 (2011) 3324−3328.

[16] J. Zhu, Z. Xia, Y. Zhang, M. S. Molokeevc, Q. Liu, Structural phase transitions and photoluminescence properties of Eu^{3+} doped $Ca_{(2-x)}Ba_xLaNbO_6$ phosphors, Dalton Trans. 44 (2015) 18536−18543.

[17] M. Sletnes, M. Lindgren, J. C. Valmalette, N. P. Wagner, T. Grande, M-A. Einarsrud, Photoluminescence of A- and B-site Eu^{3+}-substituted $(Sr_xBa_{1-x})_2CaW_yMo_{1-y}O_6$ phosphors, J. Solid State Chem. 237 (2016) 72−80.

[18] C. Wang, S. Ye, Q. Zhang, Unraveling the distinct luminescence thermal quenching behaviours of A/B-site Eu^{3+} ions in double perovskite $Sr_2CaMoO_6:Eu^{3+}$, Opt. Mater. 75 (2018) 337−346.

[19] X. Song, X. Wang, X. Xu, X. Liu, X. Ge, F. Meng, Crystal structure and magnetic-dipole emissions of Sr_2CaWO_6: RE^{3+} (RE=Dy, Sm and Eu) phosphors, J. Alloys compd. 739 (2018) 660−668.

[20] V. Sivakumar, U.V. Varadaraju, Synthesis, phase transition and photoluminescence studies on Eu^{3+}-substituted double perovskites − A novel orange-red phosphor for solid-state lighting, J. Solid State Chem. 181 (2008) 3344−3351.

[21] S. Ye, Y. Li, D. Yu, Z. Yang, Q. Zhang, Structural effects on stokes and anti-stokes luminescence of double-perovskite $(Ba,Sr)_2CaMoO_6$: Yb^{3+},Eu^{3+}, J. Appl. Phys. 110 (2011) 013517-1−013517-5.

[22] Y.-Y. Tsai, H.-R. Shih, M.-T. Tsai, Y.-S. Chang, A novel single-phased white light emitting phosphor of Eu^{3+} ions-doped Ca_2LaTaO_6, Mater. Chem. Phys. 143 (2014) 611−615.

[23] Q. Sun, S. Wang, B. Devakumar, L. Sun, J. Liang, T. Sakthivel, S. J. Dhoble, X. Huang, Double perovskite $Ca_2LuTaO_6:Eu^{3+}$ red-emitting phosphors: Synthesis, structure and photoluminescence characteristics, J. Alloys compd. 804 (2019) 230−236.

[24] S. H. Lee, Y. Cha, H. Kim, S. Lee, J. S. Yu, Luminescent properties of Eu^{3+}-activated Gd_2ZnTiO_6 double perovskite red-emitting phosphors for white light-emitting diodes and field emission displays, RCS Adv. 8 (2018) 11207−11215.

[25] N. Miniajluk, B. Bondzior, D. Stefańska, P. J. Dereń, Eu^{3+} ions in the highly symmetrical octahedral site in Ba_2MgWO_6 double perovskite, J. Alloys compd. 802 (2019) 190−195.

[26] S. C. Lal, V. Lalan, S. Ganesanpotti, Structural characterization of B-site ordered $Ba_2Ln_{2/3}TeO_6$ (Ln = La, Pr, Nd, Sm, and Eu) double perovskites and probing its luminescence as Eu^{3+} phosphor hosts, Inorg. Chem. 57 (2018) 6226−6236.

[27] C. C. Yu, X. M. Liu, M. Yu, C. K. Lin, C. X. Li, H. Wang, J. Lin, Enhanced photoluminescence of Ba_2GdNbO_6: Eu^{3+}/Dy^{3+} phosphors by Li^+ doping, J. Solid State Chem. 180 (2007) 3058−3065.

[28] R. Yu, A. Fan, T. Li, M. Yuan, J. Wang, Structure and luminescence properties of Eu^{3+}-doped trigonal double-perovskite $Ba_2Lu_{0.667}WO_6$, Mater. Chem. Phys. 196 (2017) 75−81.

[29] L. Li, W. Chang, W. Chen, Z. Feng, C. Zhao, P. Jiang, Y. Wang, X. Zhou, A. Suchocki, Double perovskite $LiLaMgWO_6$:Eu^{3+} novel red-emitting phosphors for solid state lighting: synthesis, structure and photoluminescent properties, Ceram. Int. 43 (2017) 2720−2729.

[30] A. Fu, A. Guan, F. Gao, X. Zhang, L. Zhou, Y. Meng, H. Pan, A novel double perovskite La_2ZnTiO_6:Eu^{3+} red phosphor for solid-state lighting: Synthesis and optimum luminescence, Opt. Laser Technol. 96 (2017) 43−49.

[31] Q. Liu, L. Wang, W. Huang, L. Zhang, M. Yu, Q. Zhang, Enhanced luminescence properties of double perovskite (Ba, Sr)$LaMgSbO_6:Eu^{3+}$ phosphors based on composition modulation, J. Alloys compd. 717 (2017) 156−163.

[32] J. Zhong, M. Xu, D. Chen, G. Xiao, Z. Ji, Novel red-emitting $Sr_2LaSbO_6:Eu^{3+}$ phosphor with enhanced $^5D_0 \rightarrow {}^7F_4$ transition for warm white light-emitting diodes, Dyes Pigm. 146 (2017) 272−278.

[33] W. Ran, H. M. Noh, B. K. Moon, S. H. Park, J. H. Jeong, J. H. Kim, G. Liu, J. Shi, Crystal structure, electronic structure and photoluminescence properties of $KLaMgWO_6:Eu^{3+}$ phosphors, J. Lumin. 197 (2018) 270−276.

[34] C. Wei, D. Xu, J. Li, A. Geng, X. Li, J. Sun, Synthesis and luminescence properties of Eu^{3+}-doped a novel double perovskite Sr_2YTaO_6 phosphor, J. Mater. Sci.: Mater. Electron. 30 (2019) 2864−2871.

[35] F. Fan, L. Zhao, Y. Shang, J. Liu, W. Chen, Y. Li, Thermally stable double-perovskite $Ca_3TeO_6:Eu^{3+}$ red-emitting phosphors with high color purity, J. Lumin. 211 (2019) 14−19.

[36] C. Wei, D. Xu, Z. Yang, J. Li, X. Chen, X. Li, J. Sun, Synthesis and photoluminescence properties of Eu^{3+}-Activated Double Perovskite Ba_2YTaO_6 Red Phosphor, J. Electron. Mater. 48 (2019) 5048−5054.

[37] J. Liang, B. Devakumar, L. Sun, G. Annadurai, S. Wang, Q. Sun, X. Huang, Synthesis and photoluminescence properties of a novel high-efficiency red-emitting $Ca_2LuSbO_6:Eu^{3+}$ phosphor for WLEDs, J. Lumin. 214 (2019) 116605-1−116605-7.

[38] M. Liu, B. Shen, K. Wang, J. Zhong, D. Chen, Highly efficient red-emitting $Ca_2YSbO_6:Eu^{3+}$ double perovskite phosphors for warm WLEDs, RSC Adv. 9 (2019) 20742−20748.

[39] A. R. Sharits, J. F. Khoury, P. M. Woodward, Evaluating $NaREMgWO_6$ (RE = La, Gd, Y) doubly ordered double perovskites as Eu^{3+} phosphor hosts, Inorg. Chem. 55 (2016) 12383−12390.

[40] L. Zhang, P. Han, Y. Han, Z. Lu, H. Yang, L. Wang, Q. Zhang, Structure evolution and tunable luminescence of $(Sr_{0.98-m}Ba_mEu_{0.02})_2Ca(Mo_{1-n}W_n)O_6$ phosphor with ultraviolet excitation for white LEDs, J. Alloys compd. 558 (2013) 229−235.

[41] K. Ueda, S. Tanaka, T. Yoshino, Y. Shimizu, T. Honma, Site-Selective Doping and Site-Sensitive Photoluminescence of Eu^{3+} and Tb^{3+} in Perovskite-Type $LaLuO_3$, Inorg. Chem. 58 (2019) 10890−10897.

[42] P. Dorenbos, The Eu^{3+} charge transfer energy and the relation with the band gap of compounds, J. Lumin. 111 (2005) 89-104.

[43] F. Izumi, K. Momma, Three-dimensional visualization in powder diffraction, Solid State Phenom. 130 (2007) 15−20.

[44] K. Momma, F. Izumi, VESTA3 for three dimensional visualization of crystal, volumetric and morphology data, J. Appl. Crystallogr. 44 (2011) 1272−1276.

[45] S. Geller, V. B. Bala, Crystallographic Studies of Perovskite-like Compounds. II. Rare Earth Aluminates, Acta Crystallogr. 9 (1956) 1019−1025.

[46] B. K. Agarwal, X-Ray Spectroscopy, Springer-Verlag, Berlin, 1991.

[47] G. Bunker, Introduction to XAFS, Cambridge University Press, Cambridge, 2010.

[48] C. J. Howard, B. J. Kennedy, B. C. Chakoumakos, Neutron powder diffraction study of rhombohedral rare-earth aluminates and the rhombohedral to cubic phase transition, J. Phys.: Condens. Matter 12 (2000) 349–365.

[49] P. R. Slater, J. T. Irvine, T. Ishihara, Y. Takita, High-Temperature Powder Neutron Diffraction Study of the Oxide Ion Conductor $La_{0.9}Sr_{0.1}Ga_{0.8}Mg_{0.2}O_{2.85}$, J. Solid State Chem. 139 (1998) 135-143.

[50] G. Blasse, A. Bril, On the Eu^{3+} fluorescence in mixed metal oxides. II. the $^5D_0$–$^7F_0$ emission, Philips Res. Repts. 21 (1966) 368−378.

[51] K. Ueda, S. Tanaka, R. Yamamoto, Y. Shimizu, T. Honma, F. Massuyeau, S. Jobic, Site Dependence of Tb^{3+} Luminescence in Double Perovskite-Type Alkaline Earth Lanthanum Tantalates, J. Phys. Chem. C 124 (2020) 854−860.

[52] P. M. Woodward, Octahedral tilting in perovskites. II. structure stabilizing forces, Acta Cryst. B53 (1997) 44−66.